

High-temperature spin relaxation process in $\text{Dy}_2\text{Ti}_2\text{O}_7$ probed by ^{47}Ti -NQR

K. Kitagawa,^{1,2,*} R. Higashinaka,^{2,†} K. Ishida,² Y. Maeno,² and M. Takigawa¹

¹*Institute for Solid State Physics, University of Tokyo, Kashiwanoha, Kashiwa, Chiba 277-8581, Japan*

²*Department of Physics, Graduate School of Science, Kyoto University, Kyoto 606-8502, Japan*

(Dated: June 7, 2021)

We have performed nuclear quadrupole resonance (NQR) experiments on ^{47}Ti nuclei in $\text{Dy}_2\text{Ti}_2\text{O}_7$ in the temperature range 70 – 300 K in order to investigate the dynamics of $4f$ electrons with strong Ising anisotropy. A significant change of the NQR frequency with temperature was attributed to the variation of the quadrupole moment of Dy $4f$ electrons. A quantitative account was given by the mean field analysis of the quadrupole-quadrupole (Q-Q) interaction in the presence of the crystalline-electric-field splitting. The magnitude and the temperature dependence of the nuclear spin-lattice relaxation rate was analyzed, including both the spin-spin and the Q-Q interactions. The results indicate that these two types of interaction contribute almost equally to the fluctuation of Dy magnetic moments.

PACS numbers: 76.60.-k, 75.40.Gb, 75.20.Hr

Keywords: NMR, NQR, EFG, crystal electric field, quadrupole moment, ^{47}Ti -NQR, $\text{Dy}_2\text{Ti}_2\text{O}_7$, spin ice

I. INTRODUCTION

Observation of spin relaxation in magnetic materials provides valuable information on the microscopic nature of the interactions between spins. When a system of a large spin quantum number has strong Ising anisotropy, the mutual spin-flip process is substantially depressed. The relaxation then becomes extremely slow and may eventually lead to spin freezing in real materials with competing interactions. A typical example is $\text{Dy}_2\text{Ti}_2\text{O}_7$, in which Dy^{3+} ions with large angular momentum of $J=15/2$ ($4f^9$ configuration) form a pyrochlore lattice, a network of corner-shared tetrahedra.

In $\text{Dy}_2\text{Ti}_2\text{O}_7$ (Ref. 1), as well as in other pyrochlore oxides such as $\text{Ho}_2\text{Ti}_2\text{O}_7$ (Ref. 2) and $\text{Ho}_2\text{Sn}_2\text{O}_7$ (Ref. 3), a strong crystalline electric field (CEF) forces the magnetic moments of rare earth ions to lie at low temperatures along the symmetry axis of CEF, i.e. the $[111]$ or its equivalent directions connecting the rare earth site and the center of the tetrahedron it belongs to. This strong Ising anisotropy combined with the effective ferromagnetic nearest neighbor interaction stabilizes for each bond such magnetic configurations that one moment points in and the other points out of the tetrahedron. Obviously it is not possible for all bonds to satisfy this condition. As a compromise, the ground state is selected by the rule that two moments point in and other two moments point out of every tetrahedron, which is called the “two-in, two-out” or the “ice rule”. These states are macroscopically degenerate as long as only the nearest neighbor interaction is considered. This state has been named “spin-ice” after the I_h phase of water ice, which exhibits similar degeneracy with respect to the proton configuration.

The process of spin relaxation in such a system, especially in the spin-ice state, is an interesting problem. Although the degeneracy of the spin-ice state may be eventually lifted by the long range dipolar interaction, this does not occur in real materials within an observable time scale. Thus the true ground state may never

be reached. Recently, the relaxation in $\text{Dy}_2\text{Ti}_2\text{O}_7$ and $\text{Ho}_2\text{Ti}_2\text{O}_7$ have been actively investigated by various experimental means, including the neutron spin echo experiments in $\text{Ho}_2\text{Ti}_2\text{O}_7$ (Ref. 4), the muon spin rotation measurements in $\text{Dy}_2\text{Ti}_2\text{O}_7$ (Ref. 5) and the observation of magneto-caloric effects in $\text{Dy}_2\text{Ti}_2\text{O}_7$ (Ref. 6). However, the time scale of magnetic relaxation in $\text{Dy}_2\text{Ti}_2\text{O}_7$ and $\text{Ho}_2\text{Ti}_2\text{O}_7$ varies with temperature so widely that no single experimental technique can cover the whole range.

In this paper, we report the results of nuclear magnetic resonance (NMR) and nuclear quadrupole resonance (NQR) experiments on ^{47}Ti nuclei in $\text{Dy}_2\text{Ti}_2\text{O}_7$. From the analysis of the NMR spectra in high magnetic field and at low temperatures, where the configurations of Dy spins are precisely known, we conclude that the magnetic hyperfine field at Ti nuclei is entirely due to dipolar interaction with Dy moments. The zero-field NQR measurements have been performed in the temperature range 70 – 300 K. Substantial temperature variation of the NQR frequency was attributed to the change of the quadrupole moment of Dy $4f$ electrons. A quantitative account of the data was obtained by considering both the CEF splitting and the quadrupole-quadrupole (Q-Q) interaction in a self-consistent way. The fluctuation rate ($1/\tau$) of the Dy magnetic moments extracted from the nuclear spin-lattice relaxation rate shows an activated temperature dependence. The magnitude and the T -dependence of $1/\tau$ was successfully explained by considering both the spin-spin and the Q-Q interactions, which have comparable contributions.

II. EXPERIMENT

For the ^{47}Ti -NQR/NMR experiments we have grown an isotope-enriched single crystal of $\text{Dy}_2\text{Ti}_2\text{O}_7$ using a floating-zone image furnace, starting from the sintered polycrystal containing 96% ^{47}Ti while the natural abundance of ^{47}Ti is 7.5%. The purpose of this enrichment is

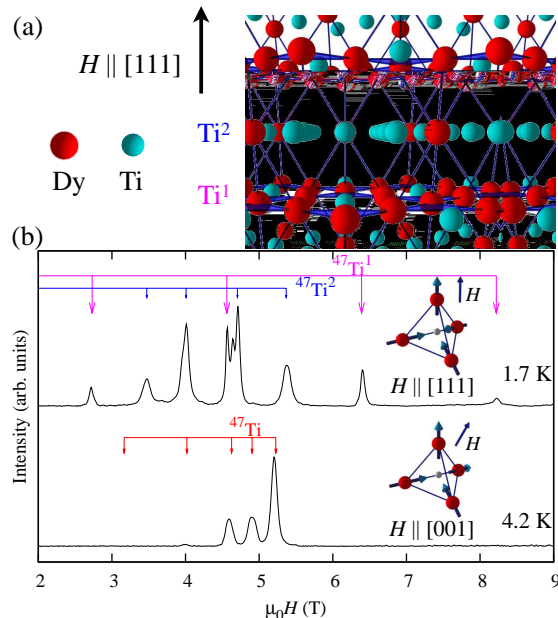


FIG. 1: (Color online) (a) The crystal structure of $\text{Dy}_2\text{Ti}_2\text{O}_7$ viewed perpendicular to the $[111]$ direction. A magnetic field applied along $[111]$ generates two spectroscopically inequivalent Ti sites; Ti^1 on the triangular plane and Ti^2 on the Kagomé plane of the Ti pyrochlore sublattice. (b) ^{47}Ti -NMR field-swept spectra at 9.7 MHz for the two field orientations. The “one-in, three-out” configuration is selected for $H \parallel [111]$, whereas the “two-in, two-out” configuration remains stable for $H \parallel [001]$. The arrows indicate the calculated resonance positions as described in the text. For $H \parallel [001]$, the two resonance lines in low field region were not observed probably because of too short T_2 .

to enhance the signal intensity and to avoid overlap of resonance lines from ^{47}Ti and ^{49}Ti , which have nearly the same gyromagnetic ratio ($^{47,49}\gamma/2\pi \simeq 2.400$ MHz/T). Since the demagnetization field of $\text{Dy}_2\text{Ti}_2\text{O}_7$ is large in high fields and at low temperatures, of the order of one tesla, the single crystal was cut into a rod extending along the $[1\bar{1}0]$ direction and the NMR coil was wound only around the central half of the rod where demagnetization field should be homogeneous.

The standard spin-echo technique was used to obtain the NMR/NQR spectra. The nuclear spin-lattice relaxation rate ($1/T_1$) was measured by NQR using the saturation recovery method. To determine $1/T_1$, the intensity of the spin-echo signal as a function of the time after the saturation pulse was fit to the theoretical formula appropriate for the specific resonance line being observed⁷. The spin-spin relaxation rate $1/T_2$ was determined by fitting the spin-echo intensity as a function of the time interval (τ) between the $\pi/2$ and the π pulses to an exponential function.

Since the NQR frequencies are relatively low (4 and 9 MHz), the long decay time of the electric ringing of the LC resonance circuit after the rf-pulses prevents obser-

TABLE I: Comparisons between the experimental and calculated resonance positions for ^{47}Ti NMR at 9.7 MHz. The calculated results are obtained by exact diagonalization of \mathcal{H}_{nuc} [Eq. (1)] with or without considering the hyperfine field from the Dy moments H_{dip} [Eq. (2)].

NMR line positions (T)					
$H \parallel [111], ^{47}\text{Ti}^1$					
Calc. w/o H_{dip}	0.382	2.218	4.042	5.872	7.701
Calc. w/ H_{dip}	0.138	2.731	4.561	6.391	8.221
Exp.		2.72	4.57	6.41	8.22
$H \parallel [111], ^{47}\text{Ti}^2$					
Calc. w/o H_{dip}	2.082	2.693	3.228	4.370	4.761
Calc. w/ H_{dip}	0.837	3.473	4.006	4.707	5.358
Exp.		3.47	4.00	4.71	5.39
$H \parallel [001], ^{47}\text{Ti}$					
Calc. w/o H_{dip}	0.941	1.536	3.735	4.360	4.423
Calc. w/ H_{dip}	3.166	4.018	4.626	4.903	5.225
Exp.			4.59	4.92	5.21

vation of the spin-echo signal for short τ . This raises a serious problem at low temperatures where T_2 becomes short. In order to overcome this difficulty, we have developed a silicon-diode-based Q-switch. This device quickly dumps the quality factor (Q) of the resonance circuit just after the irradiation of rf-pulses, allowing us to set τ as short as to 8 μs at 9 MHz.

Still the NQR experiments are not possible in a certain temperature range because of too short T_2 due to the slow dynamics of Ising spins⁸. The measurements reported in this paper are limited to high temperatures (≥ 70 K), where the spin dynamics is fast enough, or at low temperatures (≤ 4 K) and in high fields (≥ 3 T), where magnetic moments are completely aligned to certain directions by magnetic fields.

III. RESULTS AND DISCUSSION

A. High field NMR

The crystal structure of $\text{Dy}_2\text{Ti}_2\text{O}_7$ shown in Fig. 1(a) contains two pyrochlore sublattices, one formed by Ti and the other formed by Dy. A pyrochlore lattice can be viewed as the stack of alternating triangular and Kagomé planes along $[111]$. When a magnetic field applied is along $[111]$, The Ti sites on the triangular planes [Ti^1 in Fig. 1(a)] and those on the Kagomé planes (Ti^2) become inequivalent, generating distinct NMR lines. Note that Ti^1 (Ti^2) is on the Kagomé (triangular) planes of the Dy pyrochlore sublattice. When the field is applied along $[100]$, all Ti sites are equivalent. Figure 1(b) shows the NMR spectra obtained at the fixed frequency of 9.7 MHz for the two field orientations, along $[111]$ and $[100]$, at low enough temperatures. The magnetization measurements have established that at these fields and temperatures, each Dy moment of $10\mu_B$ is completely aligned to a specific direction^{9,10,11,12} as shown in the inset of Fig. 1(b).

The “one-in, three-out” or the “three-in, one-out” configuration is selected for $H \parallel [111]$, while the “two-in, two-out” configuration remains stable for $H \parallel [100]$. In the following, we demonstrate that the NMR spectra can be well reproduced by considering the dipolar field from Dy moments in these configurations.

The NMR frequencies of ^{47}Ti are determined by the following nuclear hamiltonian, which consists of the Zeeman interaction with the effective magnetic field and the nuclear quadrupole interaction with the electric field gradient (EFG)¹³,

$$\mathcal{H}_{\text{nuc}} = -\mu_0\gamma\hbar I_\alpha H_{\text{eff}}^\alpha + \frac{eQ}{6I(2I-1)}V^{\alpha\beta} \left[\frac{3}{2} (I_\alpha I_\beta + I_\beta I_\alpha) - \delta_{\alpha\beta} I^2 \right]. \quad (1)$$

Here \mathbf{I} is the nuclear spin with $I=5/2$, $Q (= 3.02 \times 10^{-29} \text{ m}^2)$ is the nuclear quadrupole moment and $V^{\alpha\beta} (= \partial^2 V / \partial r_\alpha \partial r_\beta)$ is the EFG tensor, where V is the electrostatic potential. The repeated indices of vectors and tensors should be summed over the Cartesian coordinates (Einstein’s convention).

The effective field \mathbf{H}_{eff} is the vector sum of the external field \mathbf{H} and the hyperfine field. We assume that the hyperfine field is given by the dipolar field from Dy moments.

$$H_{\text{dip}}^\alpha = \mu_B g_J \sum_j \left\{ \frac{1}{4\pi} \frac{\partial^2}{\partial r_\alpha \partial r_\beta} \left(\frac{1}{r} \right) J_\beta^{(j)} - \left(I_D - \frac{1}{3} \right) \frac{J^{\alpha;(j)}}{V_A} \right\} \quad (\text{SI}), \quad (2)$$

where μ_B is the Bohr magneton, $g_J (= 4/3)$ is the Lande’s g factor, I_D is the demagnetization factor, and V_A is the atomic volume per Dy. The direction of the saturated Dy moments J ($= 15/2$) are fixed along the local Ising axes in the low-temperature limit of our experiment. The summation over the spins j should be cut off within a sphere or performed by the Ewald’s method. We take $I_D=0.45$, which is close to the value $1/2$ for a infinitely long cylinder in horizontal fields. For $\mathbf{H} \parallel [111]$, the calculated dipolar field is $(-0.30, -0.30, -0.30)$ T at Ti^1 sites and $(-0.24, -0.24, -0.66)$ T at Ti^2 sites. For $\mathbf{H} \parallel [001]$ all Ti sites have the same dipolar field $(0.18, 0.18, -0.72)$ T.

The EFG tensors can be determined from the NQR measurements at zero magnetic field. Since the Ti sites have three-fold rotation symmetry around $[111]$, the EFG is axially symmetric, $V_{xx} = V_{yy} = -V_{zz}/2$, where $z \parallel [111]$. When $\mathbf{H}_{\text{eff}} = \mathbf{0}$, \mathcal{H}_{nuc} can be easily diagonalized to yield two NQR frequencies, $\nu_Q [\equiv 3eQ|V_{zz}|/2I(2I-1)\hbar]$ and $2\nu_Q$, corresponding to the transitions $I_z = \pm 1/2 \leftrightarrow \pm 3/2$ and $I_z = \pm 3/2 \leftrightarrow \pm 5/2$, respectively.

Now we can diagonalize \mathcal{H}_{nuc} numerically to obtain the NMR frequencies, which are the difference of the eigenvalues of \mathcal{H}_{nuc} for various transitions, as a function of external field. In order to compare the calculated results

with the experimental NMR spectra obtained by sweeping the field at a constant frequency, this function should be inverted by Newton’s method. The experimental and calculated results for the NMR line positions are compared in Fig. 1(b) and Table I. Here we used the value of $\nu_Q = 4.39$ MHz to get the best agreement. This value is very close to the observed NQR frequency at low temperatures as we describe below (Fig. 3). The results without the hyperfine field are also shown in Table I. The calculated results including the dipolar field agrees extremely well with the experimental data, demonstrating that the hyperfine coupling in $\text{Dy}_2\text{Ti}_2\text{O}_7$ is entirely due to the dipolar field. The precise knowledge of the hyperfine interaction enables us to make quantitative analysis of the NQR relaxation data we discuss later.

B. Zero field NQR

We now focus on the NQR results in zero field and at high temperatures. Figure 2 shows NQR spectra at 240 K and at 150 K. Two resonance lines are observed at ν_Q and $2\nu_Q$ as expected. However, the value of ν_Q strongly depends on temperatures, which is rather unusual. The temperature dependence of the peak frequency and the width of the NQR lines are shown in Fig 3. The value of ν_Q changes as much as 5% from 300 K to 70 K. This is an order of magnitude larger than what is expected from simple thermal contraction¹⁴. The smooth change of ν_Q and the nearly constant line width also rule out any sudden deformation of the crystal structure. A natural explanation would be that ν_Q is influenced by the change of charge density distribution of Dy $4f$ electrons due to variation of the population among the CEF split $4f$ levels. For example, Tou *et al.* reported that the temperature dependence of EFG at Sb nuclei in $\text{PrOs}_4\text{Sb}_{12}$ can be accounted for by the thermal average of the hexadecapole moments of Pr^{2+} ($4f^2$) ions which is compatible with the cubic point symmetry of the Pr sites¹⁵.

The CEF Hamiltonian \mathcal{H}_{CEF} of single Dy ion in the D_{3d} symmetry is given by the CEF parameters B_q^k and the normalized spherical harmonics $C_q^k [=$

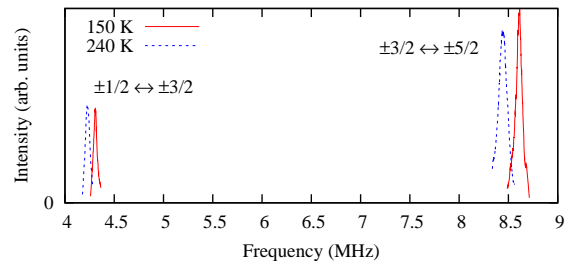


FIG. 2: (Color online) ^{47}Ti -NQR spectra at 150 K and 240 K. The NQR frequencies depend strongly on temperature.

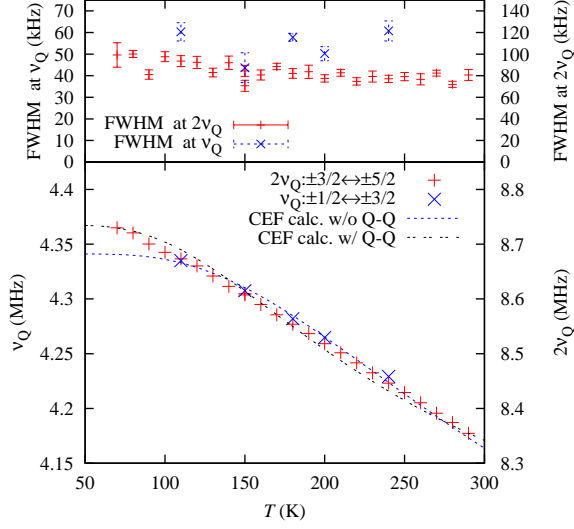


FIG. 3: (Color online) The peak frequency (lower panel) and the full width at half maximum (FWHM, upper panel) of the ^{47}Ti NQR resonance lines for the transitions $I_z = \pm 1/2 \leftrightarrow \pm 3/2$ (ν_Q) and $I_z = \pm 3/2 \leftrightarrow \pm 5/2$ ($2\nu_Q$). The dotted and double dashed lines in the lower panel show the calculated results considering the temperature dependence of the quadrupole moment $\langle C_0^2 \rangle$ without and with the electric quadrupole-quadrupole interaction, respectively.

$\sqrt{4\pi/(2k+1)}Y_q^k$ as operators.

$$\mathcal{H}_{\text{CEF}} = B_0^2 C_0^2 + B_0^4 C_0^4 + B_3^4 (C_3^4 - C_{-3}^4) + B_0^6 C_0^6 + B_3^6 (C_3^6 - C_{-3}^6) + B_6^6 (C_6^6 + C_{-6}^6). \quad (3)$$

The values of B_q^k for $\text{Ho}_2\text{Ti}_2\text{O}_7$ have been determined by Rosenkranz and co-workers¹⁶ by neutron scattering experiments. Among the family of lanthanoid titanate pyrochlores, B_q^k should change only modestly. We estimate B_q^k in $\text{Dy}_2\text{Ti}_2\text{O}_7$ by assuming the change of $\langle r^k \rangle$ for the $4f$ shells as $\langle r^k \rangle_{\text{Dy}}/\langle r^k \rangle_{\text{Ho}} = 1.05, 1.09, 1.12$ (for $k=2, 4, 6$), after Refs. 17 and 18. In order to calculate the matrix elements of C_q^k , the $|J_z\rangle$ states have to be expanded to the single-electron orbitals with the Clebsch-Gordan coefficients. The CEF level scheme for $\text{Dy}_2\text{Ti}_2\text{O}_7$ obtained by diagonalizing \mathcal{H}_{CEF} for the case of $^6H_{15/2}$ multiplet is shown in Fig. 4. Our results are in good agreement with those described in Ref. 16. Note that the CEF ground states are almost the pure $|J_z = \pm 15/2\rangle$ doublet, leading to the strong Ising anisotropy.

Since the charge distribution of $4f$ electrons is generally represented by the electric multipole moments C_q^k , it should be possible to expand ν_Q in terms of their ther-

mal average $\langle C_q^k \rangle$. Because of the D_{3d} symmetry of the Dy ions $\langle C_q^k \rangle = 0$ for $q \neq 0$. Then to the lowest order, $\nu_Q = a_0 + a_2 \langle C_0^2 \rangle + a_4 \langle C_0^4 \rangle + a_6 \langle C_0^6 \rangle$. Although the microscopic mechanism of the coupling a_k is not understood, it should include the effect of polarization of the surrounding medium. In the following we consider only the

E_i	Wave function	J_z	C_0^2
1106K	$0.814 \pm 7/2\rangle + \dots$	± 1.76	0.072
1104K	$0.952 \pm 9/2\rangle + \dots$	± 4.18	0.014
956K	$0.842 \pm 11/2\rangle + \dots$	± 3.38	-0.035
679K	$0.825 \pm 5/2\rangle + \dots$	± 2.03	0.078
547K	$0.958 \pm 3/2\rangle + \dots$	± 1.21	0.166
503K	$0.702 \pm 13/2\rangle + \dots$	± 3.61	-0.014
385K	$0.603 \pm 13/2\rangle - 0.172 \pm 7/2\rangle - 0.751 \pm 1/2\rangle + 0.110 \mp 5/2\rangle + 0.177 \mp 11/2\rangle$	± 2.54	0.042
GS	$0.986 \pm 15/2\rangle - 0.156 \pm 9/2\rangle - 0.041 \pm 3/2\rangle + 0.035 \mp 3/2\rangle + 0.007 \mp 9/2\rangle$	± 7.41	-0.323

FIG. 4: (Color online) CEF level scheme of $\text{Dy}_2\text{Ti}_2\text{O}_7$ inferred from the CEF parameters of $\text{Ho}_2\text{Ti}_2\text{O}_7$ (Ref. 16). Arrows represent the major process for the spin-flip relaxations between the ground-state doublet.

quadrupole moment and neglect the higher order multipoles,

$$\nu_Q = a_0 + a_2 \langle C_0^2 \rangle. \quad (4)$$

If we do not consider the quadrupole-quadrupole (Q-Q) interaction between neighboring Dy sites, $\langle C_0^2 \rangle$ is simply given by the Boltzman average of the expectation values of C_0^2 for the CEF eigen states,

$$\langle C_0^2 \rangle = \sum_i \frac{\langle C_0^2 \rangle_i \exp(-\beta E_i)}{Z}, \quad (5)$$

where $\beta = (k_B T)^{-1}$, and $Z = \sum_i \exp(-\beta E_i)$. The experimental data of ν_Q is fit to Eqs. (4) and (5) with the two adjustable parameters a_0 and a_2 as shown by the dotted line in Fig. 3 (labeled as “CEF calc. w/o Q-Q”). Although the experimental data are reproduced quite well above 120 K, clear deviation develops at lower temperatures. Modest change of the CEF parameters does not lead to notable improvement. In the following we demonstrate that substantial improvement can be achieved by considering the electric quadrupole-quadrupole (Q-Q) interaction in the mean field approximation.

The traceless quadrupole moment $Q_{\alpha\beta}$ in the Cartesian coordinate is defined as²⁵,

$$Q_{\alpha\beta} = -e \left(r_{\alpha} r_{\beta} - \frac{1}{3} \delta_{\alpha\beta} r^2 \right) = -\frac{1}{3} e (1 - \sigma_2) \langle r^2 \rangle \begin{pmatrix} -C_0^2 + \frac{\sqrt{6}}{2} (C_{-2}^2 + C_2^2) & -\frac{\sqrt{6}}{2} i (C_2^2 - C_{-2}^2) & -\frac{\sqrt{6}}{2} (C_1^2 - C_{-1}^2) \\ -\frac{\sqrt{6}}{2} i (C_2^2 - C_{-2}^2) & -C_0^2 - \frac{\sqrt{6}}{2} (C_{-2}^2 + C_2^2) & \frac{\sqrt{6}}{2} i (C_1^2 + C_{-1}^2) \\ -\frac{\sqrt{6}}{2} (C_1^2 - C_{-1}^2) & \frac{\sqrt{6}}{2} i (C_1^2 + C_{-1}^2) & 2C_0^2 \end{pmatrix}. \quad (6)$$

In this definition, effects of shielding is already taken into account by the Sternheimer shielding factor $\sigma_2 = 0.527$ and $\langle r^2 \rangle = 0.849$ a. u.¹⁸. From the multipole expansion of the Coulomb potentials¹⁹, the Q-Q interaction between two Dy ions is expressed as

$$\begin{aligned} \mathcal{H}_{Q-Q}^{12} &= \frac{1}{2!2!4\pi\epsilon_0} \frac{\partial^4}{\partial r_{\alpha} \partial r_{\beta} \partial r_{\gamma} \partial r_{\delta}} \left(\frac{1}{r_{12}} \right) Q_{\alpha\beta}^{(1)} Q_{\gamma\delta}^{(2)} \\ &= \frac{3}{16\pi\epsilon_0} Q_{\alpha\beta}^{(1)} Q_{\gamma\delta}^{(2)} \left(\frac{2}{r^5} \delta^{\alpha\gamma} \delta^{\beta\delta} \right. \\ &\quad \left. - \frac{20}{r^7} r^{\alpha} r^{\gamma} \delta^{\beta\delta} + \frac{35}{r^9} r^{\alpha} r^{\beta} r^{\gamma} r^{\delta} \right). \end{aligned} \quad (7)$$

It should be noted that in the formulas of the Cartesian coordinates, the operators defined on the local quantization axes have to be converted as RQR^T and $R\mathbf{J}$, where R is the rotation matrix.

The single site Hamiltonian $\mathcal{H}^{(i)}$ including both CEF and the Q-Q interaction in the mean-field approximation can be written as follows.

$$\begin{aligned} \mathcal{H}^{(i)} &= \mathcal{H}_{\text{CEF}}^{(i)} + \frac{1}{16\pi\epsilon_0} \left(C_0^{2;(i)} \langle C_0^2 \rangle - \frac{1}{2} \langle C_0^2 \rangle^2 \right) \\ &\quad \times \left[\sum_j \frac{\partial^4}{\partial r_{\alpha} \partial r_{\beta} \partial r_{\gamma} \partial r_{\delta}} \left(\frac{1}{r_{ij}} \right) \frac{\langle Q_{\gamma\delta}^{(j)} \rangle \langle Q_{\alpha\beta}^{(i)} \rangle}{\langle C_0^2 \rangle \langle C_0^2 \rangle} \right] \\ &= \mathcal{H}_{\text{CEF}}^{(i)} + (96 \text{ K}) \times \left(C_0^{2;(i)} \langle C_0^2 \rangle - \frac{1}{2} \langle C_0^2 \rangle^2 \right). \end{aligned} \quad (8)$$

The thermal average value of $\langle C_0^2 \rangle$ is calculated again from Eq. (5) but now E_i and $\langle C_0^2 \rangle_i$ are the energy and the expectation value for the eigenstates of the mean field hamiltonian, Eq. (8), which itself contains $\langle C_0^2 \rangle$ as a parameter. The temperature dependence of $\langle C_0^2 \rangle$ can then be determined self consistently by iteration. Using this result, the experimental data of ν_Q is fit to Eq. (4) as shown by the double dashed line in Fig. 3 (labeled as “CEF calc. w Q-Q”). We notice that the calculated result agrees with the experimental data much better now, in particular below 100 K. Although the Q-Q interaction is necessary to consider the high-temperature excitations, the spin-spin interaction is much more important in the low-temperature physics since the ground-state (GS) Kramers doublet has no freedom of multipole moment.

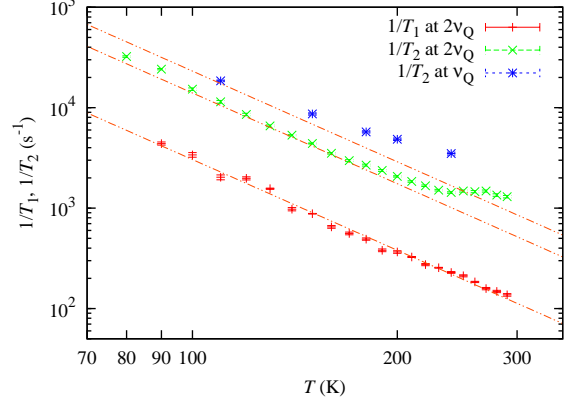


FIG. 5: (Color online) Temperature dependences of the spin-lattice relaxation rate $1/T_1$ and the spin-spin relaxation rates $1/T_2$ measured for the $I_z = \pm 1/2 \leftrightarrow \pm 3/2$ (ν_Q) and $I_z = \pm 3/2 \leftrightarrow \pm 5/2$ ($2\nu_Q$) transitions. The $1/T_1$ was measured at $2\nu_Q$. Three straight lines indicates the T^{-3} dependence. One is the fit to the data of $1/T_1$ and others are multiplied by 4.6 and 7.6 respectively (see text).

C. Spin dynamics

Let us now discuss the results of the nuclear spin-lattice relaxation rate $1/T_1$ and the nuclear spin-spin relaxation rate $1/T_2$ measured by NQR. They provide direct information on the fluctuations of Dy moments at the NQR frequencies. Figure 5 displays the temperature dependence of $1/T_1$ and $1/T_2$. For the whole temperature range, $1/T_1$ obeys the $1/T^3$ behavior remarkably well. Similar temperature dependence is observed for $1/T_2$ below 200 K. For both $1/T_1$ and $1/T_2$, the relaxation process is considered to be magnetic because relaxation rate by phononic possesses should increase with increasing temperature²⁰.

The spin-spin relaxation rate is the sum of two contributions, $1/T_2 = (1/T_2)_{\text{Dy}} + (1/T_2)_{\text{nuc}}$. The first term is due to fluctuations of Dy moments and the second term comes from the nuclear spin-spin coupling. When the fluctuations of Dy moments are much faster than the NQR frequencies, $(1/T_2)_{\text{Dy}}$ for the transition $I_z = m \leftrightarrow m+1$ is related to $1/T_1$ as

$$\left(\frac{1}{T_2} \right)_{\text{Dy}} = \frac{1}{T_1} \{ I(I+1) - m(m+1) - 1 \} + \frac{1}{T_1^{\perp}}, \quad (9)$$

This relation can be derived by extending the Walstedt's method for the transition $I_z = 1/2 \leftrightarrow -1/2$ (Ref. 21).

Here T_1^\parallel (T_1^\perp) is the relaxation time when the nuclear spin is quantized parallel (perpendicular) to z , the principal axis of EFG. Note that T_1^\parallel is equal to the actual relaxation time measured by NQR experiment. The ratio T_1^\parallel/T_1^\perp is determined by the anisotropy of the hyperfine couplings between Dy moments and a Ti nucleus.

$$\frac{T_1^\parallel}{T_1^\perp} = \frac{A_\parallel^2 + A_\perp^2}{2A_\perp^2} = 0.6. \quad (10)$$

Here, $A_\parallel = 0.0067 \text{ T}/\mu_B$ ($A_\perp = 0.019 \text{ T}/\mu_B$) for the component of the dipolar field from a single nearest Dy moment parallel (perpendicular) to z . Then, the ratio $(T_2^{-1})_{\text{Dy}}/T_1^{-1}$ should be 4.6 for $m = 1/2$ and 7.6 for $m = 3/2$. In fact, the experimental data in Fig. 5 agree with these relation below 200 K, indicating that $1/T_2$ is dominated by the spin-lattice relaxation process $(T_2^{-1})_{\text{Dy}}$. The deviation at higher temperatures is likely to be due to the temperature independent term $(1/T_2)_{\text{nuc}}$.

The rapid increase of $1/T_1$ with decreasing temperature indicates slowing down of the fluctuations of Dy moments. Basically this can be understood from the fact that the direct spin flip process is inhibited among the CEF GS doublet, which is almost purely the $|J_z = \pm 15/2\rangle$ states. Thus the spin relaxation process at high temperatures should be driven by the transitions between the GS and the excited states. If the effects of the second and higher excited states are neglected, the probability of such a process should follow the Arrhenius-type activated temperature dependence $\exp(-E_a/k_B T)$, where E_a is the energy difference between the GS and the first CEF excited states. In several experiments to date, the spin relaxation has been fitted to the Arrhenius function: the muon spin rotation and the ac-susceptibility measurements ($E_a = 210 \text{ K}$, Refs. 5 and 8), and the nuclear forward scattering experiment ($E_a = 270 \text{ K}$, Ref. 22). Although the $1/T_1$ data in Fig. 5 apparently does not fit to the Arrhenius function, we demonstrate in the following that this can be understood from the temperature dependences of both the amplitude of moment fluctuations and the fluctuation time τ , and τ does follow the Arrhenius function.

When the fluctuations of Dy moments are much faster than the NQR frequencies with short enough correlation length, $1/T_1$ is given by the Fermi's golden rule,

$$\frac{1}{T_1} = \frac{z'}{\hbar^2} ({}^{47}\gamma A_\perp g J \mu_B)^2 \langle J_z^2 \rangle \tau. \quad (11)$$

Here we consider fluctuations of only the z component of Dy moments because of the strong Ising character of the GS. The temporal correlation of J_z is assumed to be described by an exponential function $\exp(-t/\tau)$ and z' ($=6$) is the number of nearest neighbor Dy moments. The amplitude of the moment fluctuations $\langle J_z^2 \rangle$ is calculated from the CEF hamiltonian and shown in the inset of Fig. 6. The fluctuation time τ can be estimated from Eq. (11) by considering $\langle J_z^2 \rangle$ and the experimental data

of $1/T_1$, as shown in the main panel of Fig. 6 for the temperature range 100 – 300 K. In Fig. 6, τ is found to accommodate to the simple Arrhenius function with E_a of $409 \pm 10 \text{ K}$, which is close to the CEF first excitation level of 385 K. We also show the temperature dependence of τ below 100 K obtained by Sutter *et al.* from the nuclear forward scattering²². The two sets of experimental results are consistent each other within a factor of three.

The spin flip process relevant to the nuclear relaxation is illustrated by the arrows in Fig. 4. First, a Dy moment is excited from the GS to one of the the excited doublet. It then makes the transition to another state within the same excited doublet. This process is caused, for example, by the coupling $J_z^{(1)} J_+^{(2)}$, which leaves the spin state at site 1 in the GS unchanged and flips the spin at site 2 in the excited doublet. The latter process is allowed for the first excited doublet because it contains the $|\pm 1/2\rangle$ components. Finally the Dy moment in the excited state relaxes back to the GS but final state must be different from the initial state. This effectively accomplishes the spin flip in the GS: $J_z = 15/2 \leftrightarrow -15/2$. The transition within the excited doublet is required because otherwise the final state always coincides with the initial state. Below the room temperature, the population of excited states is so small that the fluctuation rate is exclusively determined by the first step.

The spin flip rate $1/2\tau$ is then given as the sum of the transition probability W from the GS to the excited states i when $E_i \gg k_B T$.

$$\frac{1}{2\tau} \sim \frac{1}{2} \sum_{i(\neq \text{GS})} W_{\text{GS} \rightarrow i}. \quad (12)$$

The factor of $1/2$ is necessary because a half of excited spins return to the original ground state without flipping. The transition probability $W_{\text{GS} \rightarrow i}$ is given by the golden rule for the mutual transition process.

$$W_{\text{GS} \rightarrow i} \sim z \frac{2\pi}{\hbar} \left| \langle \text{GS}^{(1)}, i^{(2)} | \mathcal{H}^{12} | i^{(1)}, \text{GS}^{(2)} \rangle \right|^2 \times \frac{\exp(-\beta E_i)}{Z} \frac{1}{\pi \hbar W_{i \rightarrow \text{GS}}}, \quad (13)$$

where the spin at site 2 makes transition from the GS to an excited state i while the spin at site 1 does the reverse and $z(=6)$ denotes the number of nearest-neighbor bonds. We consider the uncertainty principle that the energy width of the final state is given by the life time of the excited spin at site 2, which is $W_{i \rightarrow \text{GS}}$. From Eq. (13) and the detailed balance relation,

$$W_{\text{GS} \rightarrow i} = W_{i \rightarrow \text{GS}} \exp(-\beta E_i), \quad (14)$$

we obtain the expression for $W_{\text{GS} \rightarrow i}$ and $1/\tau$,

$$W_{\text{GS} \rightarrow i} \sim \frac{\sqrt{2z}}{\hbar} |\langle \text{GS}, i | \mathcal{H}^{12} | i, \text{GS} \rangle| \frac{\exp(-\beta E_i)}{\sqrt{Z}}, \quad (15)$$

$$\frac{1}{\tau} \sim \frac{\sqrt{2z}}{\hbar} \sum_{i(\neq \text{GS})} |\langle \text{GS}, i | \mathcal{H}^{12} | i, \text{GS} \rangle| \frac{\exp(-\beta E_i)}{\sqrt{Z}}. \quad (16)$$

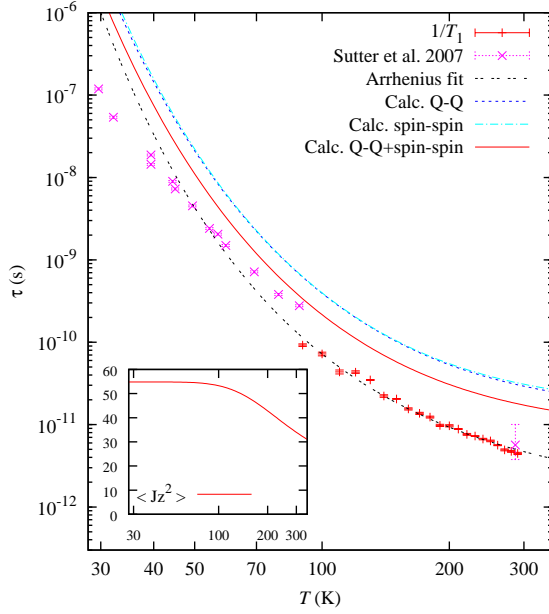


FIG. 6: (Color online) Spin relaxation time τ as a function of temperature, extracted from the ^{47}Ti -NQR relaxation rate $1/T_1$ using Eq. (11) with the amplitude of the moment fluctuation $\langle J^2 \rangle$ shown in the inset. The results of the nuclear forward scattering²² is shown for comparisons. The Arrhenius fit gives the activation energy E_a of 409 ± 10 K. The calculated results of τ based on the CEF scheme is shown for three cases, taking account of only the spin-spin interaction, only the quadrupole-quadrupole interaction, or both interactions together. The results for the first two cases coincide almost completely.

It is noted that Eq. (16) agrees with the Arrhenius behavior if the the second and the higher CEF levels are ignored.

Finally, we are at the stage to calculate $1/\tau$ in Eq. (16). The interaction between two moments \mathcal{H}^{12} , which is essential to relax the spins, is considered only between the nearest neighbors and contains of two terms: The spin-spin interaction $\mathcal{H}_{\text{spin-spin}}^{12}$ and the Q-Q interaction $\mathcal{H}_{\text{Q-Q}}^{12}$ given in Eq. (7). The spin-spin interaction consists of the antiferromagnetic exchange ($J_{\text{ex}}/3 = -1.24$ K) and ferromagnetic dipolar interactions according to the Monte Carlo study of the “dipolar spin-ice model”^{23,24},

$$\mathcal{H}_{\text{spin-spin}}^{12} = \left\{ -\frac{J_{\text{ex}}}{J^2} \delta^{\alpha\beta} + \frac{\mu_0 \mu_B^2 g_J^2}{4\pi} \frac{\partial^2}{\partial r_\alpha \partial r_\beta} \left(\frac{1}{r_{12}} \right) \right\} J_\alpha^{(1)} J_\beta^{(2)}. \quad (17)$$

The calculated results of τ are compared with the ex-

perimental results in Fig. 6. In the calculated results in, the contributions from the the spin-spin interaction and the Q-Q interaction turn out to be nearly the same. When both interactions are considered, the calculated result of τ (“Q-Q+spin-spin” in Fig. 6), agrees with the experiment reasonably well. However, there is still about a factor four difference. Possible origin for this may come from effects we have neglected such as the interactions between second nearest and further neighbors, interactions between octopoles or higher order multipoles, and short range spin correlation. However, any of those effects is difficult to estimate precisely at this moment.

In our formulation thus far, the direct-transition process between the GS is ignored just because such probability is negligibly small compared with the process we discussed in the high-temperature region. Nevertheless, the probability is not strictly zero owing to the existence of $\pm 9/2$ and $\pm 3/2$ components in the GS (Fig. 4). We consider that the direct spin flip process has to be responsible for the excitations in the spin-ice state of $\text{Dy}_2\text{Ti}_2\text{O}_7$ below 1 K, which is still not uncovered experimentally.

IV. CONCLUSION

We have investigated the Dy Ising-spin relaxation process in a range of 70 – 300 K using ^{47}Ti -NMR/NQR in $\text{Dy}_2\text{Ti}_2\text{O}_7$. The hyperfine coupling, CEF level scheme, and interaction Hamiltonians, were deduced from the low-temperature NMR spectra, experimental CEF of $\text{Ho}_2\text{Ti}_2\text{O}_7$ (Ref. 16), and the temperature dependence of the NQR frequency, respectively. Those information enabled us to calculate the absolute values of the Dy spin-flip rate and NQR relaxation rate. The absolute value of the NQR relaxation rate was analyzed in the CEF level scheme with two types of mutual spin-flip Hamiltonians: the spin-spin and Q-Q interaction. The Q-Q interaction is also necessary to account for the feature of the modification in the NQR frequency. Our experimental and calculated results reveals the spin-flip process and the importance of the Q-Q interaction in the high-temperature nature of the Ising-spins in $\text{Dy}_2\text{Ti}_2\text{O}_7$.

Acknowledgments

This work was in part supported by the Grants-in-Aid for Scientific Research from JSPS and MEXT of Japan and by the 21COE program “Center for Diversity and Universality in Physics” from MEXT of Japan.

* Electronic address: kitag@issp.u-tokyo.ac.jp

† Present affiliation: RIKEN (The Institute of Physical and

Chemical Research), Wako, Saitama 351-0198, Japan

¹ A.P.Ramirez, A.Hayashi, R.J.Cava, R.Siddharthan, and

- B.S.Shastry, Nature **399**, 333 (1999).
- ² M. J. Harris, S. T. Bramwell, D. F. McMorrow, T. Zeiske, and K. W. Godfrey, Phys. Rev. Lett **79**, 2554 (1997).
 - ³ K. Matsuhira, Y. Hinatsu, K. Tenya, and T. Sakakibara, J. Phys.: Condens. Matter **12**, L649 (2000).
 - ⁴ G. Ehlers, J. S. Gardner, C. H. Booth, M. Daniel, K. C. Kam, A. K. Cheetham, D. Antonio, H. E. Brooks, A. L. Cornelius, S. T. Bramwell, et al., Phys. Rev. B **73**, 174429 (2006).
 - ⁵ J. Lago, S. J. Blundell, and C. Baines, J. Phys: Condens. Matter **19**, 326210 (2007).
 - ⁶ M. Orendáč, J. Hanko, E. Čižmár, A. Orendáčová, M. Shirai, and S. T. Bramwell, Phys. Rev. B **75**, 104425 (2007).
 - ⁷ A. Narath, Phys. Rev. **162**, 320 (1967).
 - ⁸ J. Snyder, J. S. Slusky, R. J. Cava, and P. Schiffer, Nature **413**, 48 (2001).
 - ⁹ T. Sakakibara, T. Tayama, Z. Hiroi, K. Matsuhira, and S. Takagi, Phys. Rev. Lett. **90**, 207205 (2003).
 - ¹⁰ R. Higashinaka and Y. Maeno, Phys. Rev. Lett. **95**, 237208 (2005).
 - ¹¹ K. Matsuhira, H. Sato, T. Tayama, Z. Hiroi, S. Takagi, and T. Sakakibara, J. Phys: Condens. Matter **19**, 145269 (2007).
 - ¹² Z. Hiroi, K. Matsuhira, S. Takagi, T. Tayama, and T. Sakakibara, J. Phys. Soc. Jpn. **72**, 411 (2003).
 - ¹³ C. P. Slichter, *Principles of Magnetic Resonance* (Springer-Verlag, Berlin Heidelberg, 2002).
 - ¹⁴ H. Suzuki, F. Hata, Y. Xue, H. Kaneko, A. Hosomichi, S. Abe, R. Higashinaka, S. Nakatsuji, and Y. Maeno, unpublished. The changes of the lattice spacings from 20 K to 300 K are 0.2% according to the X-ray diffraction experiment.
 - ¹⁵ H. Tou, M. Doi, M. Sera, M. Yogi, H. Sugawara, R. Shiina, and H. Sato, J. Phys. Soc. Jpn. **74**, 2695 (2005).
 - ¹⁶ S. Rosenkranz, A. P. Ramirez, A. Hayashi, R. J. Cava, R. Siddharthan, and B. S. Shastry, J. Appl. Phys. **87**, 5914 (2000).
 - ¹⁷ A. J. Freeman and J. P. Desclaux, J. Magn. Mag. Mat. **12**, 11 (1979).
 - ¹⁸ S. Edvardsson and M. Klintenberg, J. Alloys and Compounds **275-277**, 230 (1998).
 - ¹⁹ L. Jansen, Phys. Rev. **110**, 661 (1958).
 - ²⁰ A. Abragam, *The Principles of Nuclear Magnetism* (Oxford University Press, Oxford, 1983).
 - ²¹ R. E. Walstedt, Phys. Rev. Lett. **19**, 146 (1967).
 - ²² J. P. Sutter, S. Tsutsui, R. Higashinaka, Y. Maeno, O. Leupold, and A. Q. R. Baron, Phys. Rev. B **75**, 140402(R) (2007).
 - ²³ B. C. den Hertog and M. J. P. Gingras, Phys. Rev. Lett. **84**, 3430 (2000).
 - ²⁴ R. G. Melko and M. J. P. Gingras, J. Phys: Condens. Matter **16**, R1277 (2004).
 - ²⁵ The empirical definition of $Q_{\alpha\beta}$ sometimes appears with a factor of three in literature.